



Deconstructing the Planck TT Power Spectrum to Constrain Deviations from Λ CDM

Joshua A. Kable , Graeme E. Addison , and Charles L. Bennett

Johns Hopkins University, 3400 North Charles Street, Baltimore, MD 21218, USA; jkable2@jhu.edu

Received 2020 August 4; revised 2020 October 23; accepted 2020 October 25; published 2020 December 24

Abstract

Consistency checks of Lambda cold dark matter (Λ CDM) predictions with current cosmological data sets may illuminate the types of changes needed to resolve cosmological tensions. To this end, we modify the CLASS Boltzmann code to create phenomenological amplitudes, similar to the lensing amplitude parameter A_L , for the Sachs–Wolfe, Doppler, early Integrated Sachs–Wolfe (eISW), and polarization contributions to the cosmic microwave background temperature anisotropy, and then we include these additional amplitudes in fits to the Planck TT power spectrum. We find that allowing one of these amplitudes to vary at a time results in little improvement over Λ CDM alone suggesting that each of these physical effects are being correctly accounted for given the current level of precision. Further, we find that the only pair of phenomenological amplitudes that results in a significant improvement to the fit to Planck temperature data results from varying the amplitudes of the Sachs–Wolfe and Doppler effects simultaneously. However, we show that this model is really just refinding the Λ CDM + A_L solution. We test adding our phenomenological amplitudes as well as N_{eff} , Y_{He} , and n_{run} to Λ CDM + A_L and find that none of these model extensions provide significant improvement over Λ CDM + A_L when fitting Planck temperature data. Finally, we quantify the contributions of both the eISW effect and lensing on the constraint of the physical matter density from Planck temperature data by allowing the phenomenological amplitude from each effect to vary. We find that these effects play a relatively small role (the uncertainty increases by 3.5% and 16% respectively) suggesting that the overall photon envelope has the greatest constraining power.

Unified Astronomy Thesaurus concepts: [Observational cosmology \(1146\)](#); [Cosmic microwave background radiation \(322\)](#); [Cosmological parameters \(339\)](#); [Hubble constant \(758\)](#); [Cosmological models \(337\)](#)

1. Introduction

Lambda cold dark matter (Λ CDM) is the standard model of cosmology because with only six parameters, it successfully explains a wide range of cosmological and astrophysical phenomena. However, in recent years, tensions have emerged between the preferred values of cosmological parameters resulting from fits to cosmological data sets assuming the Λ CDM model and direct measurements of those cosmological parameters. In particular, there is a 4.4σ tension in the preferred value of the Hubble constant, H_0 , between the cosmological distance ladder measurement by SH0ES, $H_0 = 74.02 \pm 1.42 \text{ km s}^{-1} \text{ Mpc}^{-1}$ (Riess et al. 2019), and the inferred value from the most precise measurements to date of the cosmic microwave background (CMB) provided by Planck, $H_0 = 67.37 \pm 0.54 \text{ km s}^{-1} \text{ Mpc}^{-1}$ (Planck Collaboration et al. 2020a).

The H_0 tension can be divided into a discordance between the preferred values by early universe observations assuming Λ CDM and direct measurements in the late universe. While this tension is usually expressed as a disagreement between Planck and the cosmological distance ladder, Addison et al. (2018) show that a similar discordance is found when combining baryon acoustic oscillation (BAO) data with Planck CMB measurements, CMB measurements from experiments other than Planck, or with primordial deuterium abundances using no CMB anisotropy data (see also, e.g., Aubourg et al. 2015; Cuceu et al. 2019; eBOSS Collaboration et al. 2020).

On the late universe side, this tension persists even if different calibrators are used for the cosmological distance ladder (Huang et al. 2020). Using the tip of the red giant branch as a calibrator results in $H_0 = 69.6 \pm 1.9 \text{ km s}^{-1} \text{ Mpc}^{-1}$ (Freedman et al. 2019), but Yuan et al. (2019) argue that this analysis overestimates the Large Magellanic Cloud extinction and instead determine

$H_0 = 72.4 \pm 2.0 \text{ km s}^{-1} \text{ Mpc}^{-1}$. Completely independent of the cosmological distance ladder, strong gravitational lensing time delays by H_0 lenses in COSMOGRAIL’s Wellspring (H0LiCOW) determine $H_0 = 73.3 \pm 1.7 \text{ km s}^{-1} \text{ Mpc}^{-1}$, which is in 3.9σ tension with Planck (Wong et al. 2020).

Because the H_0 tension exists between multiple data sets and breaks down by cosmological epoch instead of observational technique, it is unlikely to be resolved by an underestimated or unmodeled systematic, suggesting the need for physics beyond the standard model of cosmology. Finding extensions to Λ CDM that resolve the Hubble tension yet stay consistent with the multitude of cosmological data sets is challenging (see, e.g., Knox & Millea 2020). For example, it has been proposed that incorporating a form of dark energy that comprises about 10% of the energy density of the universe around matter-radiation equality and then decays away before recombination can alleviate the H_0 tension (Lin et al. 2019; Poulin et al. 2019; Berghaus & Karwal 2020). However, fitting these current early dark energy models to Planck data results in an increase in the cold dark matter density that is disfavored by large-scale structure measurements (D’Amico et al. 2020; Hill et al. 2020; Ivanov et al. 2020).

In the absence of a clear theoretical direction, it can be useful to perform consistency checks of Λ CDM predictions with current data sets to determine what kinds of changes to the standard model are necessary or even allowed (see, e.g., Kable et al. 2020; Motloch 2020). It has been shown that in addition to the H_0 tension with direct measurements, Planck data prefers a $2\text{--}3\sigma$ larger value of $S_8 = \sigma_8 \sqrt{\Omega_m/0.3}$, which measures matter clustering, than weak lensing experiments (Abbott et al. 2018; Hildebrandt et al. 2020; Joudaki et al. 2018; Hikage et al. 2019) and clustering abundance surveys (e.g., Lin & Ishak 2017; McCarthy et al. 2018).

Additionally, there is a $\sim 2.5\sigma$ tension between the preferred values of parameters like the physical cold dark matter density, ω_c , for Planck TT $\ell \leq 1000$ and Planck TT $\ell > 1000$ (or similarly for Planck TT $\ell \leq 800$ and Planck TT $\ell > 800$), which can be resolved by allowing the amplitude of the lensing contribution to the CMB TT power spectra to vary (e.g., Addison et al. 2016; Planck Collaboration et al. 2020a). This is done by extending Λ CDM to include a phenomenological amplitude, A_L , which rescales the amplitude of the lensing power spectrum as

$$C_\ell^\Psi \rightarrow A_L C_\ell^\Psi, \quad (1)$$

where A_L has a physical value of 1 (Calabrese et al. 2008). The combined Planck TT, TE, and EE power spectra prefer $A_L > 1$ at 2.8σ , which is driven largely by an improvement to the fit for multipoles $1100 \leq \ell \leq 2000$ in the Planck TT power spectrum, though there is also improvement to the fit for Planck TT $\ell < 30$ (Planck Collaboration et al. 2020a). However, the lensing power spectrum reconstructed from higher-order statistics of the Planck maps is in good agreement with standard Λ CDM predictions (e.g., Planck Collaboration et al. 2020b; Simard et al. 2018; Motloch & Hu 2020). Moreover, the South Pole Telescope Polarimeter (SPTpol) TE and EE power spectra prefer $A_L < 1$ at 1.4σ , and the Atacama Cosmology Telescope (ACT) DR4 is consistent with $A_L = 1$ within 1σ (Henning et al. 2018; Aiola et al. 2020). While the Planck TT power spectrum prefers greater peak smoothing consistent with $A_L > 1$, other cosmological data sets disfavor changing the physical amount of lensing.

In this paper, we create phenomenological amplitudes analogous to A_L for the early integrated Sachs–Wolfe (eISW), Sachs–Wolfe, Doppler, and polarization effects,¹ which all source the CMB temperature anisotropy. We fit these new phenomenological amplitudes to Planck data to determine if there are any deviations from standard Λ CDM favored by Planck. In this way, we deconstruct the TT power spectrum into its constituent sources, which provides a test for where potential model extensions are allowed or are necessary. While scaling these physical effects can affect the CMB TE power spectrum, we choose to fit only the Planck TT power spectrum as we are primarily interested in quantifying deviations from Λ CDM predictions in the temperature anisotropy, which is already known to have internal differences in the preferred Λ CDM parameter values between Planck TT $\ell \leq 800$ and Planck TT $\ell > 800$. The Planck Collaboration performed a similar exercise and found that these phenomenological amplitudes are consistent with expectations (see Footnote 30 of Planck Collaboration et al. 2020a). We quantify this consistency and extend the analysis to include combinations of the phenomenological amplitudes.

There is a well-known degeneracy in the CMB temperature data between the scalar amplitude, A_s , and the optical depth, τ . This degeneracy is broken by the reionization bump measured by $\ell \lesssim 20$ EE data (see, e.g., Figure 8 in Planck Collaboration et al. 2020c). For all cases in this paper, we include a Gaussian prior of $\tau = 0.0506 \pm 0.0086$ to account for the constraint from Planck Low ℓ EE data as described by Planck

Collaboration et al. (2020a). We tested the impact of changing both the mean value and width of the Gaussian prior on τ and found that our conclusions were insensitive to these changes.

This paper is organized as follows. In Section 2 we define the phenomenological amplitudes for the eISW, SW, Doppler, and polarization effects and discuss how each phenomenological amplitude affects the TT power spectrum. In Section 3 we show the constraints provided by the Planck 2018 TT power spectrum when we allow one or more of the phenomenological amplitudes to vary. In Section 4 we test possible extensions to Λ CDM + A_L to determine where if any further improvement in the fit can be found. Finally in Section 5, we provide conclusions.

2. The Phenomenological Amplitudes

2.1. Definitions of Phenomenological Amplitudes

In this section, we define the phenomenological amplitudes that we will use for the rest of the paper. The perturbation away from a blackbody spectrum of the CMB photon distribution, $\Theta \equiv \delta T/T$, can be quantified by integrating the various cosmological perturbations along the path of the photons. This distribution can be expanded in terms of spherical Bessel functions, j_ℓ , and wavenumbers, k , for a given perturbation as

$$\begin{aligned} \Theta_\ell(k, \eta_0) = & A_{\text{SW}} \\ & \times \int_0^{\eta_0} d\eta g(\eta) [\Theta_0(k, \eta) + \Psi(k, \eta)] j_\ell[k(\eta - \eta_0)] \\ & - A_{\text{Dop}} \int_0^{\eta_0} d\eta g(\eta) \frac{iv_b}{k} \frac{d}{d\eta} j_\ell[k(\eta - \eta_0)] \\ & + \int_0^{\eta_0} d\eta f(z(\eta), A_{\text{eISW}}) e^{-\tau} [\dot{\Psi}(k, \eta) - \dot{\Phi}(k, \eta)] j_\ell[k(\eta - \eta_0)] \\ & + A_{\text{Pol}} \int_0^{\eta_0} d\eta \left[\frac{g(\eta)\Pi}{4} + \frac{3}{4k^2} \frac{d^2}{d\eta^2} [g(\eta)\Pi] \right] j_\ell[k(\eta - \eta_0)], \end{aligned} \quad (2)$$

following Dodelson (2003). In this equation, η is conformal time, τ is the optical depth at a given conformal time, $g(\eta) \equiv -\dot{\tau}e^{-\tau}$ is the visibility function, Ψ is the Newtonian potential, Φ is the spatial perturbation to the metric, v_b is the velocity of the baryons, and Π is the polarization tensor.

The visibility function is a probability density of the conformal time when a CMB photon last scattered, so it is sharply peaked around recombination. This in turn means that the first, second, and fourth terms are sourced primarily at the surface of last scattering while the third term is sourced at all points along the way.

The first term accounts for the Sachs–Wolfe effect, which is the relative redshifting or blueshifting of CMB photons as they leave the last scattering surface due to fluctuations in the size of the gravitational potential wells. The second term accounts for the Doppler shifting of CMB photons moving toward or away from the observer along the line of sight. The third term is the contribution of the ISW effect. Much like the Sachs–Wolfe effect, this quantifies the redshifting and blueshifting of CMB photons as they climb out of and fall into gravitational potential wells; however, in this case the size of the potential wells decays because of either radiation in the early universe or dark energy in the late universe. The final term is the CMB polarization contribution to the CMB temperature anisotropy. This results from the directional dependence of Compton

¹ Note that this polarization effect refers to the the contribution to the total intensity that is sourced by CMB polarization. We define this in more detail in Section 2.

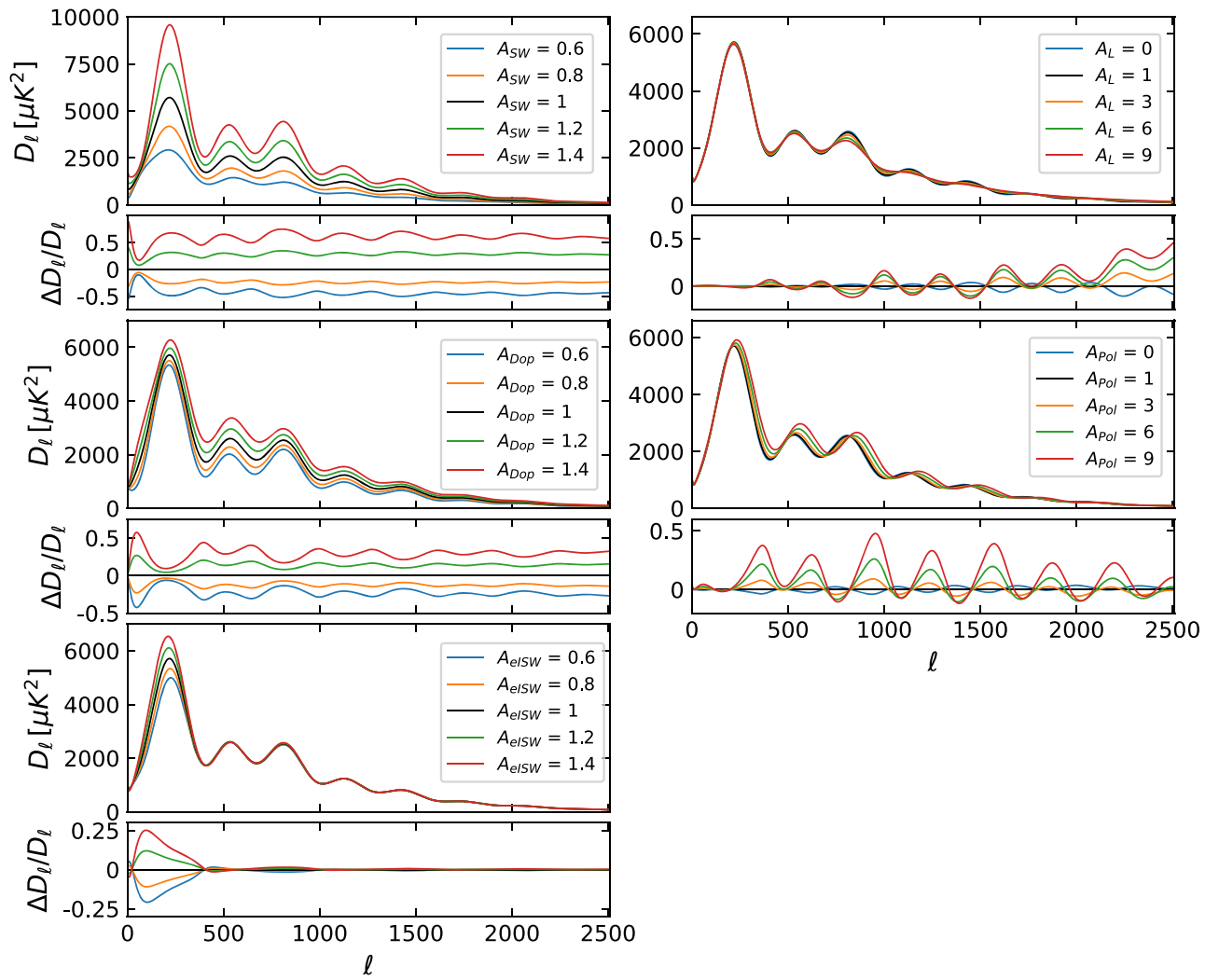


Figure 1. Impact of varying a range of phenomenological amplitudes, including A_L and the phenomenological amplitudes defined in Equation (2), while fixing the Λ CDM parameters. We additionally show the ratio of the residual with the Λ CDM case below each plot. In this paper, we examine the consistency of these amplitudes with unity as a consistency check of the standard model. If the data show a significant preference for the phenomenological amplitude not equal to unity, then this gives a clue as to what physics an alternative cosmological model would have to alter to match the data better than Λ CDM.

scattering and the coupling of the CMB polarization to the quadrupole moment of Θ , which is discussed by Hu & Sugiyama (1996).

In Equation (2), we have defined phenomenological amplitudes for each of these effects. We adopt the same convention as Hou et al. (2013) where the phenomenological amplitudes scale the sources of the photon distribution. Additionally, we define $f(z(\eta), A_{eISW}) = A_{eISW}$, when $z > 30$ and unity for $z \leq 30$ as was done in Hou et al. (2013). We could additionally define a phenomenological amplitude to account for the late time ISW effect, but we find that this is too poorly constrained by the CMB data to provide a meaningful test.

2.2. Effects of Varying Phenomenological Amplitudes on Theory TT Power Spectrum

Before we discuss results of extending Λ CDM to include these phenomenological amplitudes when fitting to Planck TT data, we illustrate the general effects on the TT power spectrum of varying each of these phenomenological amplitudes. To do so, we modify the source function in the CLASS Boltzmann code (Blas et al. 2011; Lesgourgues 2011) to include these new

parameters. In Figure 1, we show the effect on the CMB power spectrum of changing each of the four phenomenological amplitudes as well as A_L . In each case, we employ a fiducial cosmology resulting from a Markov Chain Monte Carlo (MCMC) using Monte Python (Audren et al. 2013; Brinckmann & Lesgourgues 2018) of Planck 2018 TT data with a prior of $\tau = 0.0506 \pm 0.0086$.

Changing A_{SW} has the largest effect on the overall amplitude of the power spectrum of the parameters varied in Figure 1. While increasing A_{SW} increases both acoustic peaks and troughs, it increases the heights of the peaks by a larger fraction. The effect is stronger on the compression modes (odd peaks), where the baryon-photon fluid is at the bottom of the gravitational potential, than the rarefaction modes (even peaks). Increasing the Sachs–Wolfe effect leads to deeper potentials allowing for greater compression. Increasing A_{SW} also leads to a small phase shift toward larger scales.

Increasing A_{Dop} also results in an overall increase to the power spectrum and a small phase shift to larger scales, but unlike the Sachs–Wolfe effect, it disproportionately impacts the troughs and even peaks of the power spectrum. In particular,

Table 1
Mean Values and 68% Credible Intervals for Standard Λ CDM and for Λ CDM Plus One Phenomenological Amplitude Variation for the MCMC Chains Fit to Planck TT

Parameter	Λ CDM	+ A_L	+ A_{ISW}	+ A_{Dop}	+ A_{eISW}	+ A_{Pol}
H_0	67.00 ± 0.93	69.11 ± 1.20	67.41 ± 1.03	66.90 ± 1.02	66.55 ± 0.96	67.41 ± 1.27
$100 * \omega_b$	2.213 ± 0.022	2.265 ± 0.029	2.226 ± 0.027	2.210 ± 0.030	2.170 ± 0.035	2.225 ± 0.033
ω_c	0.1205 ± 0.0021	0.1164 ± 0.0025	0.1198 ± 0.0022	0.1206 ± 0.0022	0.1206 ± 0.0021	0.1206 ± 0.0021
$10^9 A_s e^{-2\tau}$	1.8847 ± 0.0140	1.8658 ± 0.0156	1.904 ± 0.027	1.886 ± 0.022	1.873 ± 0.0165	1.8836 ± 0.0147
n_s	0.9634 ± 0.0057	0.9751 ± 0.0072	0.9666 ± 0.0067	0.9631 ± 0.0058	0.9713 ± 0.0077	0.9657 ± 0.0077
A_{new}	...	1.259 ± 0.099	0.9909 ± 0.0100	0.9984 ± 0.0126	1.064 ± 0.042	1.16 ± 0.31
$\Omega_m h^2$	0.1426 ± 0.0020	0.1390 ± 0.0023	0.1421 ± 0.0020	0.1427 ± 0.0020	0.1423 ± 0.0020	0.1428 ± 0.0020
Ω_m	0.3179 ± 0.0132	0.2915 ± 0.0148	0.3129 ± 0.0141	0.3186 ± 0.0139	0.3217 ± 0.0134	0.3147 ± 0.0148
σ_8	0.8130 ± 0.0097	0.7933 ± 0.0120	0.8147 ± 0.0099	0.8136 ± 0.0114	0.8144 ± 0.0097	0.8145 ± 0.0102
χ^2	229.50	221.45	228.59	229.49	227.24	229.18
$\chi^2_{\Lambda\text{CDM}} - \chi^2$	0	8.5	0.91	0.01	2.26	0.32

Note. For definitions of the phenomenological amplitudes see Section 2. We use a prior of $\tau = 0.0506 \pm 0.0086$.

the ratio of the heights of the peaks to troughs decreases as A_{Dop} increases. The Doppler effect is proportional to the baryon velocity as shown in Equation (2). In the absence of baryon loading, the baryon velocity would peak when $\Theta_o + \Psi = 0$, which corresponds to the troughs of the CMB power spectrum (see, e.g., Section 5.2 of Hu 1995). With the baryon loading, the baryon velocity still peaks near the troughs and therefore increasing A_{Dop} fills in the troughs. The rarefaction modes get more power than the compression modes because increasing the baryon velocity increases the pressure, which makes it easier for photons to escape the gravity wells.

Changing A_{eISW} primarily affects the first peak, but also makes small contributions to the higher peaks with a preference for the odd acoustic peaks. A_{eISW} has the largest effect on the first acoustic peak because it has the largest effect on modes that enter the horizon when the universe is dominated by matter but still has a sizable radiation density (see, e.g., Section 8.6 of Dodelson 2003). Increasing A_{eISW} causes an increase in power because it increases the radiation density, which hastens the decay of the gravity wells. There is also a slight filling in of the second trough.

Finally, Figure 1 shows that changing A_{Pol} makes the smallest change to the amplitude of the power spectrum. Increasing A_{Pol} results in a phase shift to smaller scales. This phenomenological amplitude is coupled to the CMB quadrupole moment, Θ_2 , which sources photon diffusion damping (see, e.g., Section 8.4 of Dodelson 2003). Hence, increasing A_{Pol} results in increased damping.

3. Results from Varying Phenomenological Amplitudes

In the previous section, we defined phenomenological amplitudes for the Sachs–Wolfe, eISW, Doppler, and polarization effects that source the CMB temperature anisotropy. In this section, we explore how these phenomenological amplitudes are constrained by the CMB by running MCMC fits on Planck 2018 TT data. To sample the posterior distributions for the model parameters, we use our modified CLASS Boltzmann code, which includes the amplitudes defined in Equation (2) as additional model parameters, and run MCMCs using Monte Python.

We use the likelihoods for Planck 2018 TT High ℓ Lite corresponding to $30 \leq \ell \leq 2508$ and Planck 2018 TT Low ℓ

corresponding to $\ell < 30$ provided by the Planck Collaboration. We choose to use the Lite likelihoods, where foreground parameters have already been marginalized over, because we are not investigating the impact of altering the foreground model in this work. Hereafter, we will refer to this likelihood as Planck TT.

For certain models, we also explore splitting the Planck data to highlight the discrepancy between the parameter posteriors resulting from sampling Planck TT $\ell \leq 800$ and Planck TT $\ell > 800$. We choose to split the Planck data at $\ell = 800$ because this corresponds to the point where each split of the Planck data has roughly equivalent constraining power (e.g., Planck Collaboration LI 2017). We refer to these data split likelihoods as Planck TT $\ell \leq 800$ and Planck TT $\ell > 800$, respectively.

Finally, unless otherwise specified, we use a Gelman–Rubin convergence statistic of $R - 1 = 0.05$ for the least constrained parameter to define the point when our MCMC chains have converged (Gelman & Rubin 1992).

3.1. Fits to Λ CDM Plus One Phenomenological Amplitude

In this subsection, we compare the MCMC fits to Planck TT assuming Λ CDM + one phenomenological amplitude to the MCMC fits to Planck TT assuming Λ CDM. The results of these MCMC fits are summarized in Table 1 and Figures 2 and 3. In Table 1, we show that no variations of the phenomenological amplitudes that we introduced in Section 2 are able to fit Planck TT significantly better than Λ CDM. Moreover, no variations of these phenomenological amplitudes are able to alleviate the H_0 tension.

Varying A_{eISW} results in the largest improvement over standard Λ CDM of these new phenomenological amplitudes. Nevertheless, this variation results in a $< 2\sigma$ shift in the posterior distribution for A_{eISW} away from the fiducial value of 1. Moreover, the difference in χ^2 found by adding A_{eISW} corresponds to a probability to exceed (PTE) of 0.13 further indicating that including A_{eISW} is not a significant model improvement over Λ CDM. Considering that we tested four model extensions to standard Λ CDM, it is not surprising that one of them resulted in a $> 1\sigma$ improvement to the fit.

To understand where this minor improvement is coming from, we fit Λ CDM + A_{eISW} to Planck TT but excluded multipoles $\ell < 30$ and found that the preference for $A_{\text{eISW}} > 1$

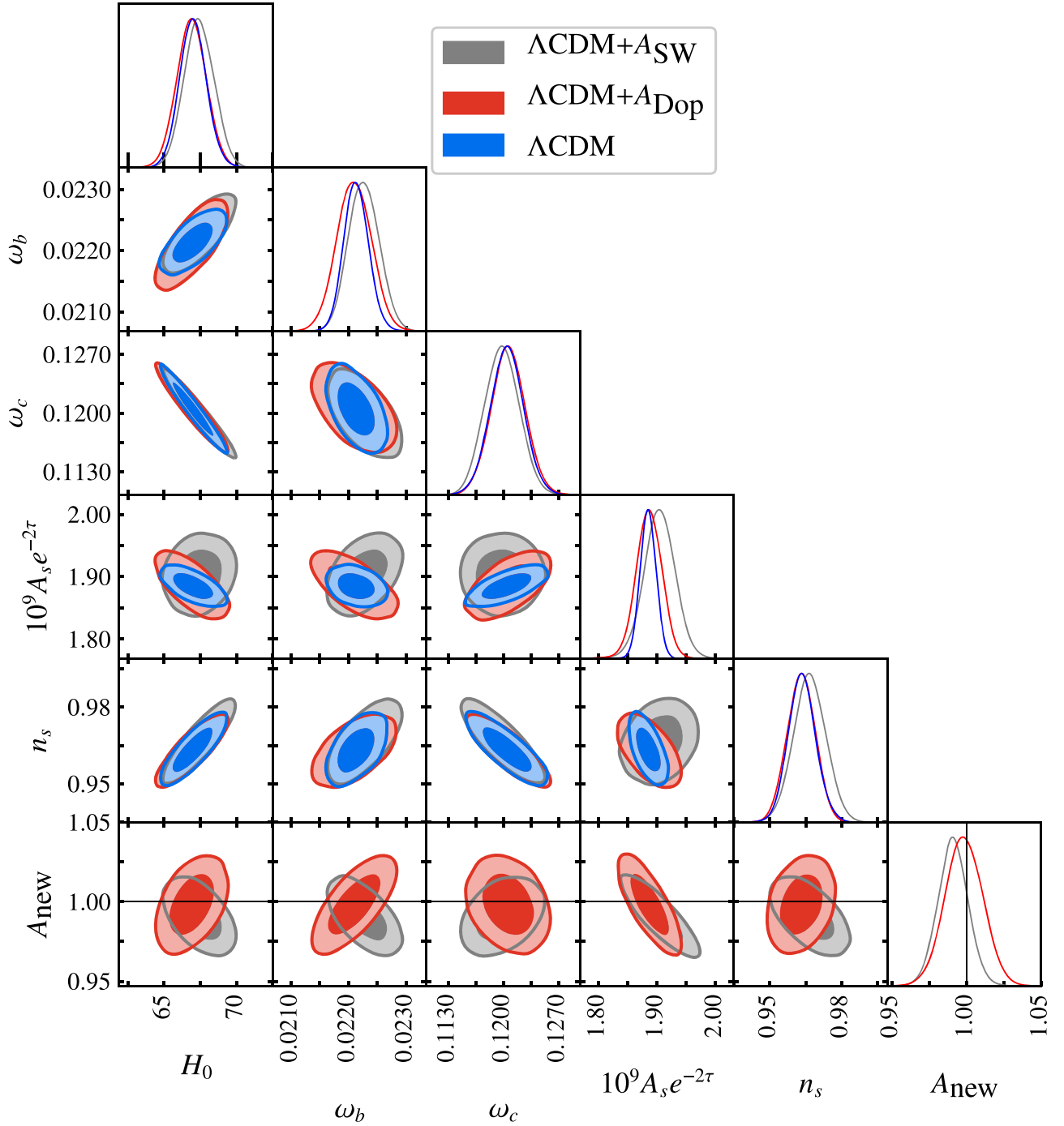


Figure 2. Posterior comparisons of Λ CDM vs. Λ CDM + A_{SW} and Λ CDM + A_{Dop} fits to Planck TT are shown. Neither phenomenological amplitude results in a significant increase in the preferred value of H_0 nor a deviation of the phenomenological amplitude from the fiducial value of 1. For ω_b , ω_c , and n_s , varying the phenomenological amplitudes keeps the Λ CDM degeneracy directions intact, but there is a clear change to the degeneracy directions involving $A_s e^{-2\tau}$. There is a difference in the sign of the degeneracy direction between A_{SW} and A_{Dop} and the cosmological parameters. This is because increasing A_{SW} disproportionately adds more power to the odd peaks and A_{Dop} disproportionately adds more power to the even peaks. In all cases a prior of $\tau = 0.0506 \pm 0.0086$ was used.

was reduced to $< 0.5\sigma$. This suggests that the primary improvement over Λ CDM when fitting Λ CDM + A_{eISW} to Planck TT comes from multipoles $\ell < 30$. In particular, we find that the TT power spectrum resulting from the best-fit cosmology for Λ CDM + A_{eISW} has less power than standard Λ CDM for $\ell < 30$ when fit to Planck TT, which allows this model to fit the well-known deficit of power at $\ell < 30$ in WMAP and Planck TT data (Bennett et al. 2013; Planck Collaboration et al. 2020a). When A_{eISW} is allowed to vary,

Planck TT prefers a decrease in the preferred value of A_s and an increase in the preferred value of n_s , which results in a reduction in power for $\ell < 30$ for the the best-fit TT power spectrum.

From Table 1, we see that the improvement found by Λ CDM + A_{eISW} over standard Λ CDM is primarily compensated by a 0.043 shift downward in the value of $100 * \omega_b$ (100 times the physical baryon density), which corresponds to almost twice the original uncertainty. On a related note, the uncertainty of the baryon density

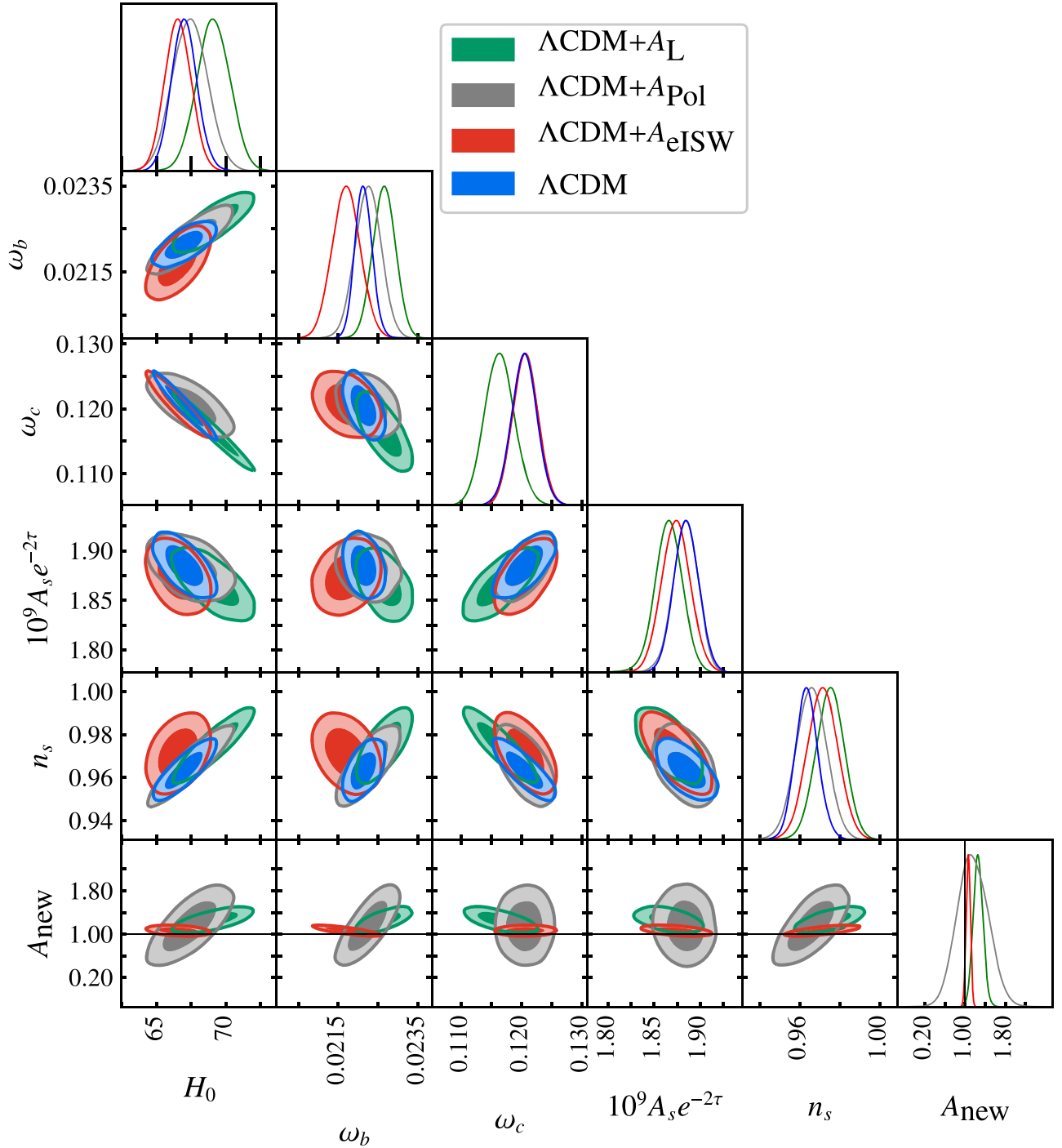


Figure 3. Posterior comparisons of Λ CDM vs. Λ CDM + A_L , Λ CDM + A_{eISW} , and Λ CDM + A_{Pol} fits to Planck TT. The Planck TT data prefer $A_{eISW} > 1$ at $>1\sigma$ and $A_L > 1$ at $>2\sigma$. Note that varying either of these two phenomenological amplitudes tends to shift the baryon density, ω_b , in opposite directions as seen by the orthogonal degeneracy directions. Varying A_{Pol} results in significant degradation in the overall Λ CDM parameter precision, which can be seen most clearly in the greater than 30% increase in the error in H_0 and the 50% increase in the error on ω_b . In all cases a prior of $\tau = 0.0506 \pm 0.0086$ was used.

when varying the amplitude of the eISW effect increases by roughly 60%, which illuminates how powerful the relative peak heights, and in particular the height of the first acoustic peak, are in constraining the physical baryon density.

After A_L and A_{eISW} , allowing A_{SW} to vary results in the next most significant improvement over just Λ CDM, which can be seen by the approximately 1σ shift in the value of A_{SW} from the fiducial value of unity. While the uncertainties on the Λ CDM parameters increase, such as the near doubling of the uncertainty

of $A_s e^{-2\tau}$, most parameter shifts are $<0.5\sigma$. Adding A_{Dop} to Λ CDM when fitting Planck TT results in a $<0.5\sigma$ shift of the posterior distribution of A_{Dop} from the fiducial value of unity. From a phenomenological perspective, these tests provide no significant evidence for an improvement over Λ CDM by solely modifying the monopole or dipole contributions to the CMB photon distribution.

The Λ CDM + A_{Pol} fit to Planck TT generally results in no substantial shifts in the central value of the posteriors. The

Table 2
Mean Values and 68% Credible Intervals Λ CDM Plus One or More Phenomenological Amplitudes for the MCMC Chains Fit to Planck 2018 TT Full ℓ

Parameter	+ A_L	+ A_{SW}	+ A_{Dop}	+ A_{eISW}	+ $A_{SW} + A_{Dop}$	+ $A_{SW} + A_{Dop} + A_{eISW}$
H_0	69.11 \pm 1.20	67.41 \pm 1.03	66.90 \pm 1.02	66.55 \pm 0.96	67.52 \pm 1.04	68.59 \pm 1.46
100 * ω_b	2.265 \pm 0.029	2.226 \pm 0.027	2.210 \pm 0.030	2.170 \pm 0.035	2.180 \pm 0.032	2.225 \pm 0.054
ω_c	0.1164 \pm 0.0025	0.1198 \pm 0.0022	0.1206 \pm 0.0022	0.1206 \pm 0.0021	0.1187 \pm 0.0023	0.1173 \pm 0.0026
$10^9 A_s e^{-2\tau}$	1.8658 \pm 0.0156	1.904 \pm 0.027	1.886 \pm 0.022	1.873 \pm 0.0165	2.145 \pm 0.107	2.32 \pm 0.20
n_s	0.9751 \pm 0.0072	0.9666 \pm 0.0067	0.9631 \pm 0.0058	0.9713 \pm 0.0077	0.9786 \pm 0.0084	0.9783 \pm 0.0085
A_L	1.259 \pm 0.099
A_{SW}	...	0.9909 \pm 0.0100	0.936 \pm 0.023	0.903 \pm 0.039
A_{Dop}	0.9984 \pm 0.0126	...	0.925 \pm 0.029	0.890 \pm 0.043
A_{eISW}	1.064 \pm 0.042	...	0.929 \pm 0.067
$\Omega_m h^2$	0.1390 \pm 0.0023	0.1421 \pm 0.0020	0.1427 \pm 0.0020	0.1423 \pm 0.0020	0.1405 \pm 0.0022	0.1395 \pm 0.0023
Ω_m	0.2915 \pm 0.0148	0.3129 \pm 0.0141	0.3186 \pm 0.0139	0.3217 \pm 0.0134	0.3085 \pm 0.0140	0.2972 \pm 0.0172
σ_8	0.7933 \pm 0.0120	0.8147 \pm 0.0099	0.8136 \pm 0.0114	0.8144 \pm 0.00978	0.865 \pm 0.023	0.891 \pm 0.033
χ^2	221.45	228.59	229.49	227.24	222.53	220.33
$\chi^2_{\Lambda\text{CDM}} - \chi^2$	8.5	0.91	0.01	2.26	6.97	9.17

Note. For definitions of the phenomenological amplitudes see Section 2. We use a prior of $\tau = 0.0506 \pm 0.0086$.

largest such shift is a 0.41 km s⁻¹ Mpc⁻¹ shift upward in the mean value of H_0 . Nevertheless there are substantial increases in the uncertainties of the parameters over the Λ CDM case. In particular, note that the uncertainties of H_0 and ω_b increase by roughly 35% and 50%, respectively, over the Λ CDM case. This highlights the importance of the polarization effect even when determining parameters from the TT spectrum.

In Figure 2 we compare the two-dimensional posterior distributions for Λ CDM + either A_{SW} or A_{Dop} to the Λ CDM case. The correlations between either A_{SW} or A_{Dop} and the Λ CDM parameters have an opposite sign for these two models because these phenomenological amplitudes disproportionately add power to either odd or even acoustic peaks of the power spectrum as discussed in Section 2. For example, increasing A_{SW} disproportionately adds power to the odd peaks which must then be compensated by decreasing the baryon density. In contrast, increasing A_{Dop} disproportionately adds power to even peaks, which must then be compensated for by increasing the baryon density. In Figure 3, we show the constraints for Λ CDM and Λ CDM + one of A_L , A_{eISW} , or A_{Pol} . In all of these cases, the size of the contours increase dramatically over Λ CDM, which should be contrasted with the relatively minor changes when varying either A_{SW} or A_{Dop} .

In summary, these tests show that Λ CDM is able to correctly account for the Sachs–Wolfe, eISW, Doppler, and polarization effects measured by Planck with the known caveat that there is an internal tension in the Planck data between low ℓ and high ℓ , which can be relieved by allowing a parameter like A_L to vary. Because the cosmological parameters do not shift much when the amplitudes for the Sachs–Wolfe, Doppler, eISW, or polarization effects are varied, the parameter constraints from these physical processes are internally consistent. Finally we note that even when allowing the amplitudes for any one of the physical effects that source the CMB temperature anisotropy to vary, Planck TT is still able to place strong constraints on the Λ CDM parameters.

3.2. Λ CDM + $A_{SW} + A_{Dop}$

In the previous subsection, we showed results for extending Λ CDM to include one of the phenomenological amplitudes that we introduced in Section 2. In this subsection, we discuss

adding pairs of the phenomenological amplitudes. In general, we find that much like adding one phenomenological amplitude, adding pairs of phenomenological amplitudes does not result in either an improved fit to Planck TT or a reduction in the H_0 tension with late universe measurements. We find that only Λ CDM + $A_{SW} + A_{Dop}$ exhibits a significant improvement to the fit to Planck TT.

We summarize the results of the MCMC sampling for Λ CDM + $A_{SW} + A_{Dop}$ to Planck TT in Table 2. With two parameters, it becomes more complicated to define when there is a significant shift in the posterior, but A_{SW} and A_{Dop} are both more than 2σ below the fiducial value of unity when simultaneously allowed to vary. Additionally, the PTE of the $\Delta\chi^2$ assuming two degrees of freedom is 0.03 indicating a significant improvement over the Λ CDM case. Note that adding both A_{SW} and A_{Dop} together results in a significant improvement over standard Λ CDM when fitting to Planck TT because when only one at a time was added there was much less improvement. Allowing both A_{SW} and A_{Dop} to vary simultaneously does not also increase the Planck TT preferred value of H_0 like when adding A_L .

Note that since A_{SW} and A_{Dop} appear to be acting in unison, we should recover approximately the same model if we use a single phenomenological amplitude to scale both the Sachs–Wolfe and Doppler effects. Taking a step back, if we had used a single amplitude to rescale all of the effects that source the CMB TT anisotropy in Equation (2), then this new phenomenological amplitude would have been almost completely degenerate with A_s , up to corrections from lensing, when fitting to Planck TT. In this case, A_s becomes a proxy for A_L because of how A_s explicitly enters the equations for lensing (see, e.g., Sections 3.1–3.2 of Lewis & Challinor 2006). Varying both A_{SW} and A_{Dop} simultaneously increases the uncertainty of $A_s e^{-2\tau}$ by a factor of 4 relative to the Λ CDM case, which allows sufficient freedom for A_s to become a proxy for A_L .

Additionally in Table 2, we include the constraints when A_{eISW} is added to Λ CDM + $A_{SW} + A_{Dop}$. For this MCMC run, we only used a convergence criteria of $R - 1 = 0.1$ because convergence was difficult to achieve. While this Λ CDM + $A_{SW} + A_{Dop} + A_{eISW}$ result gives a significant improvement over Λ CDM with a PTE of 0.03 assuming a $\Delta\chi^2$ with three degrees of freedom, it is

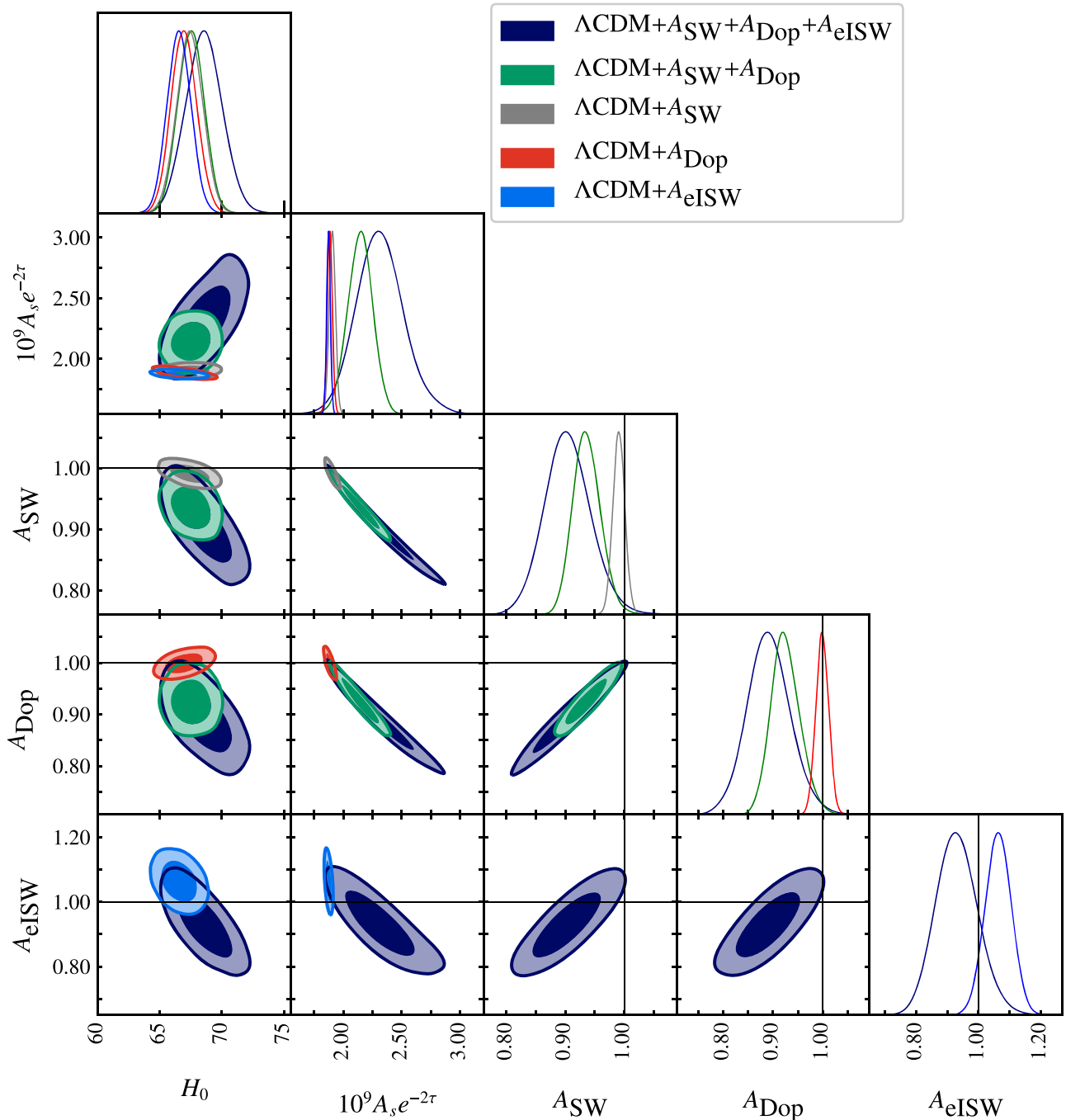


Figure 4. Posteriors of $\Lambda\text{CDM} + A_{\text{SW}} + A_{\text{Dop}} + A_{\text{eISW}}$, $\Lambda\text{CDM} + A_{\text{SW}} + A_{\text{Dop}}$, $\Lambda\text{CDM} + A_{\text{SW}}$, $\Lambda\text{CDM} + A_{\text{Dop}}$, and $\Lambda\text{CDM} + A_{\text{eISW}}$ fits to Planck TT. Including both A_{SW} and A_{Dop} results in a strong degeneracy between the phenomenological amplitudes and $A_s e^{-2\tau}$ which was not necessarily expected given the posteriors when only one of them is varied. The model $\Lambda\text{CDM} + A_{\text{SW}} + A_{\text{Dop}}$ prefers values for A_{SW} and A_{Dop} that deviate from unity by about 2σ . Additionally including A_{eISW} results in an even stronger degeneracy between the phenomenological amplitudes and A_s , which notably broadens the allowed parameter space for parameters like H_0 . Nevertheless, the result is still consistent with $A_{\text{eISW}} = 1$, which suggests that adding A_{eISW} does not result in a significant improvement over $\Lambda\text{CDM} + A_{\text{SW}} + A_{\text{Dop}}$. In all cases there is a prior of $\tau = 0.0506 \pm 0.0086$.

not a significant improvement over $\Lambda\text{CDM} + A_{\text{SW}} + A_{\text{Dop}}$ with a PTE of 0.13 assuming one degree of freedom. This improved $\Delta\chi^2$ is roughly equivalent to the improved $\Delta\chi^2$ when adding only A_{eISW} to ΛCDM as shown in Table 1, but note that Planck TT prefers $A_{\text{eISW}} < 1$ for this model to be more in line with the preferred values for A_{SW} and A_{Dop} . While adding A_{eISW} to $\Lambda\text{CDM} + A_{\text{SW}} + A_{\text{Dop}}$ does not result in a significant improvement, there is an increase in the preferred value of H_0 similar to the $\Lambda\text{CDM} + A_L$ preferred H_0 value.

In Figure 4, we compare the 2D posteriors for the one parameter extensions, $\Lambda\text{CDM} + A_{\text{SW}}$, A_{Dop} , and A_{eISW} , and the combinations $\Lambda\text{CDM} + A_{\text{SW}} + A_{\text{Dop}}$ and $\Lambda\text{CDM} + A_{\text{SW}} + A_{\text{Dop}} + A_{\text{eISW}}$. Note the strong degeneracies between the phenomenological amplitudes and the scalar amplitude when more than one phenomenological amplitude is varied. Adding A_{eISW} results in a substantial increase in the degeneracy between the phenomenological amplitudes and the scalar amplitude. This, in turn, allows for parameters like H_0 to access a broader parameter space.

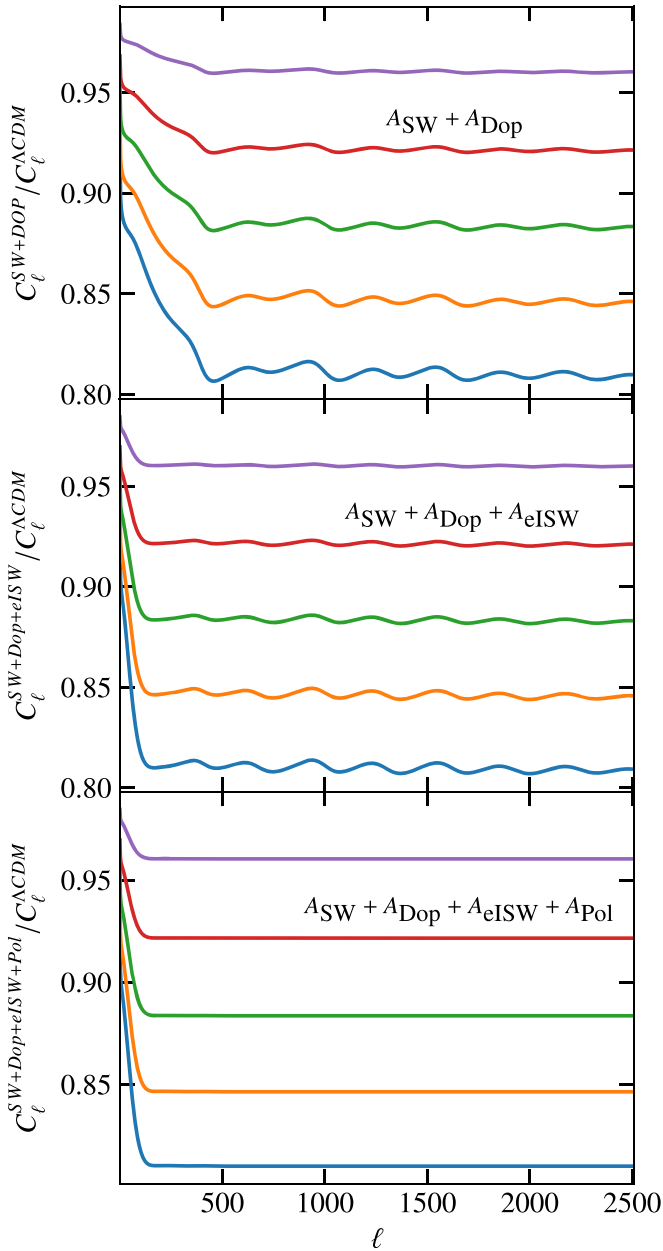


Figure 5. Top panel: ratio of the TT power spectrum when varying both A_{SW} and A_{Dop} together to the TT power spectrum of standard ΛCDM . The curves correspond to all phenomenological amplitudes being set to $\{0.90, 0.92, 0.94, 0.96, 0.98\}$ from top to bottom. If A_{SW} and A_{Dop} act in unison, then, at high ℓ , they can rescale the power spectrum and allow A_s to become a proxy for A_L , which results in a significant improvement over ΛCDM by mimicking the effect of lensing. Middle panel: when A_{eISW} acts in unison with A_{SW} and A_{Dop} the degeneracy extends to lower multipole moments resulting in a stronger degeneracy. Bottom panel: the wiggles at high ℓ result from not including A_{Pol} in the rescaling.

In Figure 5, we demonstrate how the Sachs–Wolfe and Doppler effects work together to rescale the power spectrum by plotting the quotient of the $\Lambda\text{CDM} + A_{\text{SW}} + A_{\text{Dop}}$ case to the ΛCDM case. In particular note that for $\ell > 400$, the quotient is flat, up to some wiggles that result from not additionally rescaling A_{Pol} . In the middle panel of Figure 5, we show that the slope in the quotient for $\ell < 400$ results from not also rescaling the ISW effect. For $\Lambda\text{CDM} + A_{\text{SW}} + A_{\text{Dop}}$, it is this ability to rescale the TT power spectrum on scales $\ell > 400$ that

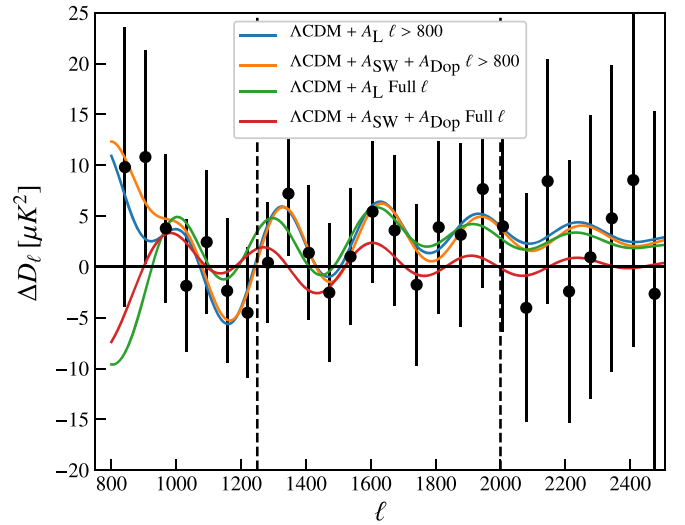


Figure 6. Residuals of the best-fit TT power spectrum from $\Lambda\text{CDM} + A_L$ and $\Lambda\text{CDM} + A_{\text{SW}} + A_{\text{Dop}}$ fits to both Planck TT and Planck TT $\ell > 800$ with the ΛCDM fit to Planck TT. We additionally include the residual of the measured Planck TT data (black) points, but we have rebinned them with $\Delta\ell \approx 65$ for visual clarity. When fit to only Planck TT $\ell > 800$, varying the amplitudes for the Sachs–Wolfe and Doppler effects results in a similar residual to the $\Lambda\text{CDM} + A_L$ residual, which suggests that at high ℓ these two models achieve approximately the same effect. The $\Lambda\text{CDM} + A_{\text{SW}} + A_{\text{Dop}}$ fit to Planck TT is restricted predominantly by the ISW effect breaking the degeneracy between the A_{SW} , A_{Dop} , and A_s , but it still fits the oscillatory residual in the multipole range $1250 \leq \ell \leq 2000$, which explains the improved fit to the χ^2 over the ΛCDM fit to Planck TT. Note that the bins provided by the Planck collaboration for Plik Lite are highly correlated at high ℓ .

degrades the precision of A_s allowing it to become a proxy for A_L .

Because the degeneracy between A_{SW} , A_{Dop} , and A_s when fitting $\Lambda\text{CDM} + A_{\text{SW}} + A_{\text{Dop}}$ breaks down for multipoles $\ell < 400$, we use fits to Planck TT and Planck TT $\ell > 800$ to illustrate that $\Lambda\text{CDM} + A_{\text{SW}} + A_{\text{Dop}}$ is approximately finding the $\Lambda\text{CDM} + A_L$ solution. In Figure 6, we show the residuals of the theory TT power spectrum calculated using the best-fit parameters for the $\Lambda\text{CDM} + A_L$ and $\Lambda\text{CDM} + A_{\text{SW}} + A_{\text{Dop}}$ fits to both Planck TT and Planck TT $\ell > 800$ with the theory TT power spectrum calculated using the best-fit parameters for the ΛCDM fit to Planck TT. Additionally, we include the residual of the measured Planck TT data with the ΛCDM fit to Planck TT. To increase the clarity of the plot, we rebin the Planck TT data using new super bins of $\Delta\ell \approx 65$. Note that there are high levels of correlation, often at the 80% level, between the bins for Plik Lite, which result from marginalizing over the foregrounds.

Importantly, Figure 6 shows that the residuals for $\Lambda\text{CDM} + A_L$ and $\Lambda\text{CDM} + A_{\text{SW}} + A_{\text{Dop}}$ are highly correlated when fit to Planck TT $\ell > 800$, which emphasizes that these two models are making the same changes at high ℓ , and it is the low ℓ behavior that restricts the latter model when fit to Planck TT. For $\ell > 1250$, the $\Lambda\text{CDM} + A_L$ fit to Planck TT also becomes highly correlated to these fits indicating that this is the primary feature of the lensing solution. Further note that the $\Lambda\text{CDM} + A_{\text{SW}} + A_{\text{Dop}}$ fit to Planck TT does fit the oscillatory residual in the Planck data, albeit without the increased power for multipoles $\ell > 1250$. This is how the $\Lambda\text{CDM} + A_{\text{SW}} + A_{\text{Dop}}$ fit to Planck TT achieves a significant improvement over ΛCDM .

In Table 3, we show the results from MCMC runs for ΛCDM , $\Lambda\text{CDM} + A_L$, and $\Lambda\text{CDM} + A_{\text{SW}} + A_{\text{Dop}}$ fits to Planck TT $\ell \leq 800$ and Planck TT $\ell > 800$. Neither $\Lambda\text{CDM} + A_L$ nor

Table 3Mean Values and 68% Credible Intervals for Λ CDM, Λ CDM + A_L , and Λ CDM + $A_{\text{SW}} + A_{\text{Dop}}$ MCMC Chains Fits to Planck 2018 TT $\ell \leq 800$ and $\ell > 800$

Parameter	Λ CDM $\ell \leq 800$	$A_L \ell \leq 800$	$A_{\text{SW}} + A_{\text{Dop}} \ell \leq 800$	Λ CDM $\ell > 800$	$A_L \ell > 800$	$A_{\text{SW}} + A_{\text{Dop}} \ell > 800$
H_0	69.95 ± 1.84	71.1 ± 2.1	73.3 ± 5.0	64.28 ± 1.33	71.0 ± 4.8	69.93 ± 5.3
$100 * \omega_b$	2.252 ± 0.042	2.283 ± 0.050	2.345 ± 0.111	2.193 ± 0.039	2.387 ± 0.145	2.273 ± 0.145
ω_c	0.1145 ± 0.0033	0.1128 ± 0.0036	0.1106 ± 0.0068	0.1279 ± 0.0034	0.1152 ± 0.0088	0.1162 ± 0.0106
$10^9 A_s e^{-2\tau}$	1.8559 ± 0.0170	1.8477 ± 0.0177	1.80 ± 0.31	1.922 ± 0.021	1.896 ± 0.025	2.59 ± 0.62
n_s	0.9756 ± 0.0120	0.9829 ± 0.0137	0.9895 ± 0.0186	0.9489 ± 0.0119	0.9579 ± 0.0134	0.9823 ± 0.037
A_L	...	1.64 ± 0.53	1.41 ± 0.30	...
A_{SW}	1.014 ± 0.073	0.873 ± 0.115
A_{Dop}	1.045 ± 0.104	0.858 ± 0.142
$\Omega_m h^2$	0.1370 ± 0.0030	0.1355 ± 0.0032	0.1341 ± 0.0053	0.1498 ± 0.0033	0.1390 ± 0.0075	0.1389 ± 0.0099
Ω_m	0.281 ± 0.021	0.269 ± 0.022	0.255 ± 0.049	0.363 ± 0.023	0.282 ± 0.053	0.292 ± 0.067
σ_8	0.7858 ± 0.0139	0.7789 ± 0.0150	0.758 ± 0.087	0.8371 ± 0.0124	0.783 ± 0.040	0.923 ± 0.086
χ^2	95.48	94.04	94.35	123.28	121.10	121.32

Note. For definitions of the phenomenological amplitudes see Section 2. We use a prior of $\tau = 0.0506 \pm 0.0086$.

Λ CDM + $A_{\text{SW}} + A_{\text{Dop}}$ results in a significantly better fit to the Planck temperature data when only half of the data are included. This highlights that the improvement found when allowing either A_L or A_{SW} and A_{Dop} to vary is primarily in bringing the two halves of the Planck power spectrum into better agreement.

Allowing A_{SW} and A_{Dop} to vary when fitting to either Planck TT $\ell \leq 800$ or Planck TT $\ell > 800$ results in an increase in the preferred value of H_0 , though notably the uncertainty of H_0 also increases to be $>5 \text{ km s}^{-1} \text{ Mpc}^{-1}$. For Planck TT $\ell > 800$, the uncertainty on H_0 increases by a factor of 3.7 when A_L is allowed to vary indicating that lensing is important in constraining cosmological parameters at high ℓ .

In summary, we find that adding the phenomenological amplitudes we introduced in Section 2 in pairs does not result in a significant improvement to the fit to Planck TT over standard Λ CDM. The one exception is when the phenomenological amplitudes for the Sachs–Wolfe and Doppler effects are both allowed to vary, but we show that this solution is really approximately refinding the Λ CDM + A_L solution by allowing A_s to become a proxy for A_L . Adding more phenomenological amplitudes, such as A_{eISW} , can make this approximation marginally better but does not result in a significant improvement to the fit to Planck TT.

4. Can Additional Model Freedom Improve over Λ CDM + A_L ?

In the previous section we found that none of the phenomenological amplitudes that we introduced in Section 2 showed any significant deviations from standard Λ CDM predictions. Moreover, while we found that combining the phenomenological amplitudes for the Sachs–Wolfe and Doppler effects show a $\sim 2.7\sigma$ preference for A_{SW} and A_{Dop} both below unity, we noted that this solution was just refinding the Λ CDM + A_L solution.

In this section we test some extensions to Λ CDM + A_L to seek a model extension that better fits Planck TT. In Section 4.1, we test extending the Λ CDM + A_L model to include the phenomenological amplitudes that we introduced in Section 2. In Section 4.2, we test extending the Λ CDM + A_L model to include one of N_{eff} , n_{run} , and Y_{He} , which all have effects on the high multipole moments of the TT power spectrum.

4.1. Testing A_L Plus One Additional Phenomenological Amplitude

In this subsection, we add the phenomenological amplitudes introduced in Section 2 to Λ CDM + A_L and fit to Planck TT. While the results in Section 3.1 showed no preference for any of these phenomenological amplitudes alone, Section 3.2 highlights the possibility that multiple phenomenological amplitudes working together could result in some improvement to the fit to Planck TT.

The results of adding A_{SW} , A_{Dop} , A_{eISW} , or A_{Pol} to Λ CDM + A_L when fitting to Planck TT are summarized in Table 4. From Table 4, it is clear that there is almost no improvement to the χ^2 when including these phenomenological amplitudes. Moreover, none of the posteriors for the phenomenological amplitudes are more than 1σ away from unity. This is consistent with our results from Section 3.1 but again highlights that each of these physical effects are being correctly accounted for.

In Section 3.1, we showed that Λ CDM + A_{eISW} results in a minor improvement of 2.26 in the χ^2 fit to Planck TT over Λ CDM alone. Adding A_{eISW} to Λ CDM + A_L results in almost no change in the χ^2 from the Λ CDM + A_L case nor a significant shift in the preferred value of A_{eISW} from unity. This suggests that the changes made by varying A_{eISW} are no longer necessary when A_L is already allowed to vary. This is consistent with the primary improvement to the fit to Planck TT found in the Λ CDM + A_{eISW} model coming from multipoles $\ell < 30$ as Λ CDM + A_L already makes improvements to fitting these multipoles. Note that the improvement in the multipole range $\ell < 30$ when Λ CDM + A_L is fit to Planck TT results from freeing up the constraints on other cosmological parameters such as allowing the preferred value of A_s to decrease and the preferred value of n_s to increase.

The model Λ CDM + A_L + A_{eISW} also provides an exploration into how the physical matter density is constrained by the CMB TT power spectrum. Knox & Millea (2020) point out that the physical matter density is predominantly determined by the overall photon envelope, followed by lensing, and then finally by the eISW effect. When A_L is allowed to vary, the uncertainty of the physical matter density increases by roughly 16.5% over standard Λ CDM. Meanwhile, allowing A_{eISW} to vary results in a 3.5% increase in the uncertainty over standard Λ CDM. Allowing A_L and A_{eISW} to vary results in a

Table 4
Mean Values and 68% Credible Intervals for Λ CDM + A_L Plus One Phenomenological Parameter for the MCMC Chains Fit to Planck 2018 TT Full ℓ

Parameter	+ A_L	+ $A_L + A_{SW}$	+ $A_L + A_{Dop}$	+ $A_L + A_{eISW}$	+ $A_L + A_{Pol}$
H_0	69.11 \pm 1.20	69.04 \pm 1.20	68.87 \pm 1.23	69.02 \pm 1.39	69.45 \pm 1.55
100 * ω_b	2.265 \pm 0.029	2.259 \pm 0.030	2.248 \pm 0.035	2.258 \pm 0.051	2.274 \pm 0.040
ω_c	0.1164 \pm 0.0025	0.1162 \pm 0.0025	0.1165 \pm 0.0025	0.1164 \pm 0.0026	0.1165 \pm 0.0025
$10^9 A_s e^{-2\tau}$	1.8658 \pm 0.0156	1.838 \pm 0.036	1.880 \pm 0.024	1.8643 \pm 0.0169	1.8635 \pm 0.0176
n_s	0.9751 \pm 0.0072	0.9736 \pm 0.0073	0.9748 \pm 0.0072	0.9761 \pm 0.0080	0.9768 \pm 0.0090
A_L	1.259 \pm 0.099	1.329 \pm 0.126	1.286 \pm 0.105	1.258 \pm 0.111	1.263 \pm 0.100
A_{new}	...	1.0116 \pm 0.0128	0.9874 \pm 0.0137	1.009 \pm 0.047	1.13 \pm 0.36
$\Omega_m h^2$	0.1390 \pm 0.0023	0.1388 \pm 0.0023	0.1389 \pm 0.0023	0.1390 \pm 0.0023	0.1392 \pm 0.0023
Ω_m	0.2915 \pm 0.0148	0.2917 \pm 0.0148	0.2934 \pm 0.0151	0.2923 \pm 0.0164	0.2892 \pm 0.0161
σ_8	0.7933 \pm 0.0120	0.7866 \pm 0.0141	0.7973 \pm 0.0128	0.7938 \pm 0.0129	0.7939 \pm 0.0127
χ^2	221.45	220.98	220.72	221.44	221.40
$\chi^2_{\Lambda\text{CDM}+A_L} - \chi^2$	0	0.47	0.73	0.01	0.05

Note. For definitions of the phenomenological amplitudes see Section 2. We use a prior of $\tau = 0.0506 \pm 0.0086$.

Table 5
Mean Values and 68% Credible Intervals for Λ CDM + A_L Plus One of N_{eff} , Y_{He} , and n_{run} for the MCMC Chains Fit to Planck TT

Parameter	+ A_L	+ $A_L + N_{\text{eff}}$	+ $A_L + n_{\text{run}}$	+ $A_L + Y_{\text{He}}$
H_0	69.11 \pm 1.20	71.5 \pm 3.8	69.14 \pm 1.19	69.70 \pm 1.49
100 * ω_b	2.265 \pm 0.029	2.293 \pm 0.052	2.271 \pm 0.031	2.283 \pm 0.040
ω_c	0.1164 \pm 0.0025	0.1187 \pm 0.0046	0.1164 \pm 0.0025	0.1156 \pm 0.0027
$10^9 A_s e^{-2\tau}$	1.8658 \pm 0.0156	1.8770 \pm 0.0157	1.8688 \pm 0.0165	1.8696 \pm 0.0170
n_s	0.9751 \pm 0.0072	0.987 \pm 0.020	0.9744 \pm 0.0072	0.9822 \pm 0.0122
A_L	1.259 \pm 0.099	1.302 \pm 0.117	1.270 \pm 0.099	1.287 \pm 0.107
N_{eff}	...	3.30 \pm 0.40
n_{run}	-0.0050 \pm 0.0076	...
Y_{He}	0.261 \pm 0.020
$\Omega_m h^2$	0.1390 \pm 0.0023	0.1415 \pm 0.0048	0.1391 \pm 0.0023	0.1384 \pm 0.0024
Ω_m	0.2915 \pm 0.0148	0.279 \pm 0.025	0.2915 \pm 0.0147	0.2856 \pm 0.0169
σ_8	0.7933 \pm 0.0120	0.7992 \pm 0.0157	0.7931 \pm 0.0122	0.7936 \pm 0.0124
χ^2	221.45	220.91	221.14	220.99
$\chi^2_{\Lambda\text{CDM}+A_L} - \chi^2$	0	0.54	0.31	0.46

Note. We use a prior of $\tau = 0.0506 \pm 0.0086$.

19% increase in the physical matter density over standard Λ CDM. This suggests that the overall photon envelope constrains the physical matter density significantly more than either lensing or the eISW effect, consistent with Knox & Millea (2020). However, note that Table 3 shows that allowing A_L to vary results in a 240% increase in the uncertainty of the physical matter density when only $\ell > 800$ are included. This highlights the importance of lensing to constraining the physical matter density at high ℓ .

Note that Λ CDM + A_L + A_{Dop} shows the largest reduction in the χ^2 despite the fact that adding A_{Dop} to Λ CDM resulted in the smallest change to the χ^2 . This is accompanied by a 0.92σ shift downward in preferred value of A_{Dop} , both of which indicate that this is not a significant improvement. The preferred value of A_{SW} for the model Λ CDM + A_L + A_{SW} shifts upward by about 0.9σ , comparable to the shift in the preferred value of A_{Dop} . Adding either A_{SW} or A_{Dop} to Λ CDM + A_L results in either more power to the odd peaks or similarly less power to the even peaks. In both cases, the preferred value of A_L is able to increase relative to the preferred value of A_L from Λ CDM + A_L fit to Planck TT data.

Allowing both A_L and A_{Pol} to vary results in a negligible shift in the central values of the posteriors and a negligible improvement to the χ^2 when fitting to Planck TT data. Again, the most significant effect when allowing A_{Pol} to vary is an increase in the uncertainty of parameters such as the 30% increase in the uncertainty of H_0 .

4.2. Testing A_L Plus One Additional Nonphenomenological Amplitude

In this subsection we test models for Λ CDM + A_L + one of N_{eff} , n_{run} , and Y_{He} . N_{eff} is designed to account for the effective number of relativistic degrees of freedom well after electron-positron annihilation. The parameter n_{run} accounts for possible linear order deviations from a flat primordial power spectrum with a spectral tilt given by n_s . Finally, the helium fraction, Y_{He} , affects the free electron density before and during recombination. All of these parameters added to Λ CDM + A_L could in principle affect the low ℓ and high ℓ consistency.

The results of adding N_{eff} , n_{run} , or Y_{He} to Λ CDM + A_L when fitting to Planck TT data are shown in Table 5. From Table 5, it

is clear that none of these result in a significant improvement to the fit. There is an increase of about $2.4 \text{ km s}^{-1} \text{ Mpc}^{-1}$ in the preferred value of H_0 when allowing both A_L and N_{eff} to vary. This is accompanied by a roughly 300% increase in the uncertainty of H_0 placing the posterior for H_0 within 1σ of the measured value by the cosmological distance ladder. However, when the Planck TE and EE power spectra are added to the fit, the constraint becomes $H_0 = 68.1 \pm 1.7 \text{ km s}^{-1} \text{ Mpc}^{-1}$, which corresponds to a 2.7σ tension with the distance ladder preferred value for H_0 . Therefore, $\Lambda\text{CDM} + A_L + N_{\text{eff}}$ is not a plausible resolution of the Hubble tension.

In this section, we have allowed various additional types of model freedom but found no substantial improvement over $\Lambda\text{CDM} + A_L$; for whatever reason A_L does seem to do a very effective job at relieving internal Planck tension.

5. Conclusions

We test the impact of allowing phenomenological amplitudes for the Sachs–Wolfe, eISW, Doppler, and polarization effects, which source the CMB temperature anisotropy, to vary when fitting to the Planck TT power spectrum. We find that allowing these amplitudes to vary results in only minimal improvement in the fit over standard ΛCDM . Moreover, there are only minimal shifts in the preferred values of the ΛCDM parameters when the amplitudes of these physical effects are varied. We conclude that ΛCDM correctly accounts for each of these physical effects.

Additionally, we test allowing multiple of these phenomenological amplitudes to vary simultaneously and find that allowing A_{SW} and A_{Dop} to vary together was the only combination that results in a significant improvement to the χ^2 when fitting to Planck TT data. However, we also show that allowing these two phenomenological amplitudes to vary simultaneously results in a significant degradation of the precision of A_s , which comes from the near rescaling of the power spectrum for multipoles $\ell > 400$ when A_{SW} and A_{Dop} are scaled in unison. When only multipoles $\ell > 800$ are included in the fit to the Planck TT spectrum, $\Lambda\text{CDM} + A_{\text{SW}} + A_{\text{Dop}}$ produces almost the same power spectrum as $\Lambda\text{CDM} + A_L$. We conclude that $\Lambda\text{CDM} + A_{\text{SW}} + A_{\text{Dop}}$ is finding the $\Lambda\text{CDM} + A_L$ solution and therefore does not provide any new evidence for deviations from ΛCDM predictions.

From our tests where we vary A_L and A_{eISW} both simultaneously and separately, we quantitatively determine that the physical matter density is constrained primarily by the overall photon envelope with smaller contributions from both lensing and the eISW effect when fitting to Planck TT data. These findings are in line with Knox & Millea (2020). However, when only Planck TT $\ell > 800$ data is included, lensing provides the majority of the constraining power for the physical matter density.

Finally, we varied both A_L and one of N_{eff} , n_{run} , and Y_{He} and fit to Planck TT data. All of these parameters impact the TT power spectrum at high ℓ meaning each of these parameter extensions provides a test of whether A_L is fully able to resolve the internal tension between Planck TT $\ell \leq 800$ and Planck TT $\ell > 800$. We find no significant improvement in the fit over the $\Lambda\text{CDM} + A_L$ case, which suggests that there is little room for improvement from each of these effects.

Allowing these phenomenological amplitudes for the physical effects that source the CMB temperature anisotropy to vary provides a new test of consistency of each of these physical effects with ΛCDM predictions. While none of our

new phenomenological tests provide evidence for deviations in the predictions made by ΛCDM , this lack of deviations from ΛCDM highlights that ΛCDM is generally good at describing the very complex nature of the CMB temperature anisotropy with the caveat that there is a known Planck internal tension between $\ell \leq 800$ and $\ell > 800$. These tests suggest that any new model of cosmology will need to make similar predictions to ΛCDM for the Sachs–Wolfe, Doppler, eISW, and polarization effects.

This work was supported in part by NASA ROSES grants NNX17AF34G and 80NSSC19K0526. We acknowledge the use of the Legacy Archive for Microwave Background Data Analysis (LAMBDA), part of the High Energy Astrophysics Science Archive Center (HEASARC). HEASARC/LAMBDA is a service of the Astrophysics Science Division at the NASA Goddard Space Flight Center. This research project was conducted using computational resources at the Maryland Advanced Research Computing Center (MARCC). This work is based on observations obtained with Planck (<http://www.esa.int/Planck>), an ESA science mission with instruments and contributions directly funded by ESA Member States, NASA, and Canada. Figures 2, 3, and 4 were created using the Python package GetDist (Lewis 2019). We thank Janet Weiland and Mario Aguilar Faúndez for helpful comments while completing the write up of this work.

ORCID iDs

Joshua A. Kable  <https://orcid.org/0000-0002-0516-6216>
 Graeme E. Addison  <https://orcid.org/0000-0002-2147-2248>
 Charles L. Bennett  <https://orcid.org/0000-0001-8839-7206>

References

- Abbott, T. M. C., Abdalla, F. B., Alarcon, A., et al. 2018, *PhRvD*, **98**, 043526
- Addison, G. E., Huang, Y., Watts, D. J., et al. 2016, *ApJ*, **818**, 132
- Addison, G. E., Watts, D. J., Bennett, C. L., et al. 2018, *ApJ*, **853**, 119
- Aiola, S., Calabrese, E., Maurin, L., et al. 2020, arXiv:2007.07288
- Aubourg, É., Bailey, S., Bautista, J. E., et al. 2015, *PhRvD*, **92**, 123516
- Audren, B., Lesgourgues, J., Benabed, K., & Prunet, S. 2013, *JCAP*, **2013**, 001
- Bennett, C. L., Larson, D., Weiland, J. L., et al. 2013, *ApJS*, **208**, 20
- Berghaus, K. V., & Karwal, T. 2020, *PhRvD*, **101**, 083537
- Blas, D., Lesgourgues, J., & Tram, T. 2011, *JCAP*, **2011**, 034
- Brinckmann, T., & Lesgourgues, J. 2018, arXiv:1804.07261
- Calabrese, E., Slosar, A., Melchiorri, A., Smoot, G. F., & Zahn, O. 2008, *PhRvD*, **77**, 123531
- Cuceu, A., Farr, J., Lemos, P., & Font-Ribera, A. 2019, *JCAP*, **2019**, 044
- D’Amico, G., Senatore, L., Zhang, P., & Zheng, H. 2020, arXiv:2006.12420
- Dodelson, S. 2003, *Modern Cosmology* (Amsterdam: Academic Press)
- eBOSS Collaboration, Alam, S., Aubert, M., et al. 2020, arXiv:2007.08991
- Freedman, W. L., Madore, B. F., Hatt, D., et al. 2019, *ApJ*, **882**, 34
- Gelman, A., & Rubin, D. B. 1992, *StaSc*, **7**, 457
- Henning, J. W., Sayre, J. T., Reichardt, C. L., et al. 2018, *ApJ*, **852**, 97
- Hikage, C., Oguri, M., Hamana, T., et al. 2019, *PASJ*, **71**, 43
- Hildebrandt, H., Köhlinger, F., van den Busch, J. L., et al. 2020, *A&A*, **633**, A69
- Hill, J. C., McDonough, E., Toomey, M. W., & Alexander, S. 2020, *PhRvD*, **102**, 043507
- Hou, Z., Keisler, R., Knox, L., Millea, M., & Reichardt, C. 2013, *PhRvD*, **87**, 083008
- Hu, W. 1995, arXiv:astro-ph/9508126
- Hu, W., & Sugiyama, N. 1996, *ApJ*, **471**, 542
- Huang, C. D., Riess, A. G., Yuan, W., et al. 2020, *ApJ*, **889**, 5
- Ivanov, M. M., McDonough, E., Hill, J. C., et al. 2020, *PhRvD*, **102**, 103502
- Joudaki, S., Blake, C., Johnson, A., et al. 2018, *MNRAS*, **474**, 4894
- Kable, J. A., Addison, G. E., & Bennett, C. L. 2020, *ApJ*, **888**, 26
- Knox, L., & Millea, M. 2020, *PhRvD*, **101**, 043533

- Lesgourgues, J. 2011, arXiv:1104.2932
- Lewis, A. 2019, arXiv:1910.13970
- Lewis, A., & Challinor, A. 2006, *PhR*, 429, 1
- Lin, M.-X., Benevento, G., Hu, W., & Raveri, M. 2019, *PhRvD*, 100, 063542
- Lin, W., & Ishak, M. 2017, *PhRvD*, 96, 083532
- McCarthy, I. G., Bird, S., Schaye, J., et al. 2018, *MNRAS*, 476, 2999
- Motloch, P. 2020, *PhRvD*, 101, 123509
- Motloch, P., & Hu, W. 2020, *PhRvD*, 101, 083515
- Planck Collaboration LI 2017, *A&A*, 607, A95
- Planck Collaboration, Aghanim, N., Akrami, Y., et al. 2020a, *A&A*, 641, A6
- Planck Collaboration, Aghanim, N., Akrami, Y., et al. 2020b, *A&A*, 641, A8
- Planck Collaboration, Aghanim, N., Akrami, Y., et al. 2020c, *A&A*, 641, A5
- Poulin, V., Smith, T. L., Karwal, T., & Kamionkowski, M. 2019, *PhRvL*, 122, 221301
- Riess, A. G., Casertano, S., Yuan, W., Macri, L. M., & Scolnic, D. 2019, *ApJ*, 876, 85
- Simard, G., Omori, Y., Aylor, K., et al. 2018, *ApJ*, 860, 137
- Wong, K. C., Suyu, S. H., Chen, G. C. F., et al. 2020, *MNRAS*, 498, 1420
- Yuan, W., Riess, A. G., Macri, L. M., Casertano, S., & Scolnic, D. 2019, *ApJ*, 886, 61